Hollow Fiber Gas Permeator with Counter-Current and Co-Current Flow: Series Solutions

ARTICLE *in* INDUSTRIAL & ENGINEERING CHEMISTRY FUNDAMENTALS · MAY 1986

DOI: 10.1021/i100022a007

3 AUTHORS, INCLUDING:

Noureddine Boucif
University of Lorraine
9 PUBLICATIONS **82** CITATIONS
SEE PROFILE

Kamalesh Sirkar
New Jersey Institute of Technology
201 PUBLICATIONS **5,533** CITATIONS
SEE PROFILE

Hollow Fiber Gas Permeator with Countercurrent or Cocurrent Flow: Series Solutions

Noureddine Boucif, Amitava Sengupta, and Kamalesh K. Sirkar*

Department of Chemistry and Chemical Engineering, Stevens Institute of Technology, Hoboken, New Jersey 07030

The problems in the numerical solution of boundary value problems encountered in hollow fiber binary gas permeators having cocurrent or countercurrent permeate flow with axial pressure drop inside the fiber bore are discussed. A series solution technique is developed to express each product composition and the pressure ratio as a power series in terms of a dimensionless membrane area for shell side constant-pressure feed flow. Cocurrent or countercurrent rating or design problems require the solution of either one algebraic equation, two coupled algebraic equations, or three coupled algebraic equations to determine the unknown quantities of interest. Calculated product and reject compositions, stage cuts, and closed-end pressure ratios compare quite well with those from numerical solutions for practically useful low to moderate cuts over a wide range of parameters. Cocurrent rating calculations requiring solution of only one algebraic equation are recommended for shortcut procedures since flow pattern effects are significant but not large.

Introduction

Gas separation by selective permeation through a nonporous polymeric membrane is now being commercially achieved by either a hollow fiber or a spirally wound permeator. Among the two membrane configurations, the hollow fiber geometry is utilized in the two most commercially successful devices, e.g., the PRISM separator of Monsanto (Maclean and Graham, 1980) and the cellulose ester hollow fiber permeators of Dow. These devices are being increasingly utilized for H_2 recovery, acid gas removal, CO_2 recovery for enhanced oil recovery applications, etc., in preference to conventional gas separation processes. Consequently, there exists a need for rapid and accurate hollow fiber permeator design procedures since exact numerical solutions not only consume considerable computer time but are highly prone to convergence problems (Antonson et al., 1977). The need for analytical or semianalytical solutions is further appreciated when computer simulation of a number of interconnected process units is required for preliminary process design purposes.

Commercial hollow fiber gas permeators process fluid mixtures at moderate to high pressure. The mixture usually flows outside the hollow fibers, permeate pressure buildup occurring inside the fiber bore. As indicated by Pan and Habgood (1978), the boundary conditions at either end of the fiber will not be completely known a priori. A trial and error method was adopted by them to solve the boundary value problem numerically for permeation separation of a binary feed mixture in cocurrent or countercurrent flow on the shell side of the rigid hollow fiber module. This paper develops an approximate solution for the same boundary value problem arising out of either countercurrent or cocurrent flow patterns. The only difference between our problem and that treated in Pan and Habgood (1978) lies in our neglect of the fiber lengths embedded in the tube sheets.

The binary gas separation by a hollow fiber permeator considered here assumes constant species permeability as in Pan and Habgood (1978). We note that Chern et al. (1984) have numerically studied concentration-dependent species permeability by using a dual-mode model. We are also not concerned here with the effect of fiber deformation in a hollow fiber permeator, the latter having been studied experimentally by Stern et al. (1977) for externally pressurized silicone rubber capillaries. Binary gas separation with internally pressurized silicone rubber capillaries has been experimentally and numerically investigated by Thorman et al. (1975). Although hollow fiber deformation is significant in the last two studies using a rubbery polymer, their effect is expected to be minor for hollow fibers of rigid glassy polymers used in commercial permeators.

In this paper, a series solution in terms of a nondimensional membrane area is developed for both the permeate and reject compositions, as well as for the pressure in the fiber bore. The method has been applied to both countercurrent as well as cocurrent flow pattern. This study is an extension of the series solution technique used earlier by Boucif et al. (1984) for a binary gas permeator with no axial pressure drop in either stream. As in Boucif et al. (1984), the series solutions obtained herein have been compared with the numerical solutions of the governing equations and the range of validity of the approximate solutions has been identified.

The approximate solution technique proposed here is general in nature. Concentration-dependent permeabilities, sweep gases, asymmetric membranes, etc., can be incorporated if necessary. The solution method may also be extended to the rapid approximate design of gas permeators separating a ternary feed mixture.

Governing Equations for Cocurrent and Countercurrent Hollow Fiber Gas Permeator

Consider Figure 1, a and b, illustrating the hollow fiber permeators under consideration for cocurrent and countercurrent flow patterns, respectively. For simplicity, only a single hollow fiber has been shown in each permeator. High-pressure feed gas of more permeable component 1 mole fraction x_f and molar flow rate L_f enters on the shell side outside the fibers at a pressure P_f. A high-pressure reject stream having a more permeable component 1 mole fraction x_w and molar flow rate L_w leaves the shell at the other end. The hollow fiber has an active section of length l_w through which permeation takes place. The inactive sections of the hollow fiber are embedded in the tube sheets at two ends. No permeation takes place through these lengths. The permeated stream with a more permeable component mole fraction y_w leaves the hollow fiber bore with a molar flow rate of V_w and a pressure of p_w for the cocurrent scheme of Figure 1a. For the coun-

0196-4313/86/1025-0217$01.50/0

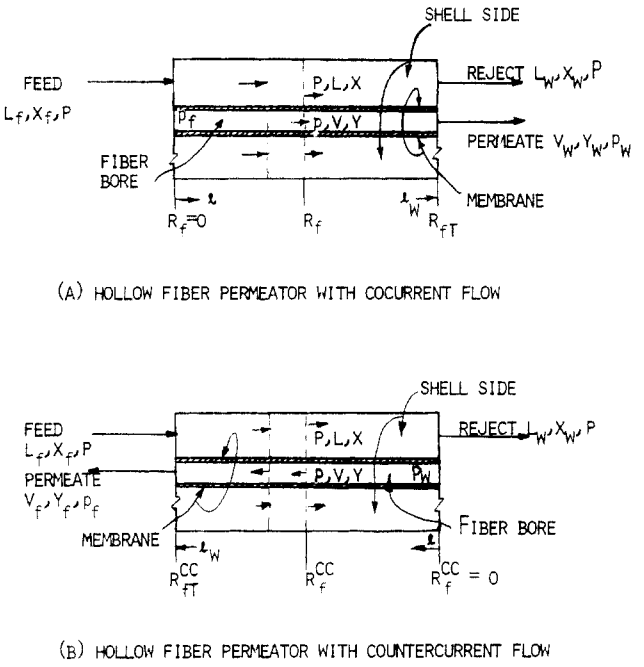

Figure 1. Schematic of a hollow fiber gas permeator having feed on the shell side and permeate inside the fiber bore in (a) cocurrent flow or (b) countercurrent flow.

tercurrent scheme of Figure 1b, the permeated stream of mole fraction y_f and molar flow rate of V_f leaves the hollow fiber bore at a pressure of p_f.

In each flow pattern, the local pressure p and the local more permeable component 1 mole fraction y of the permeate stream inside the fiber bore vary from one end to the other. Normally the exit pressure in each flow pattern is specified, i.e., p_f in countercurrent flow and p_w in cocurrent flow. In a real permeator, these pressures will correspond to those at the exit end of the inactive section of fiber embedded in the tube sheet. In our analysis, we neglect the pressure drop in the flow of the permeate gas through the inactive section of the fiber. Consequently, the specified exit pressures will correspond to those at the end of the active section of the hollow fiber. These and other assumptions used here are as follows:

1. The feed gas pressure on the shell side is constant at the value P_f.
2. The permeability of each gas species is constant.
3. Laminar flow exists inside the fiber, and the Poiseuille equation may be used for pressure drop estimation along with ideal gas behavior.
4. No axial or transverse diffusion occurs in the gas phases.
5. No purge stream is being used.
6. The viscosity of the gas mixture is assumed to be independent of pressure and composition.
7. There is no permeate stream pressure drop in the inactive sections of the fiber bore.
8. For membrane surface area and thickness (δ) in the governing equations, the outside diameter D_o is to be replaced by the logarithmic mean diameter $D_{lm} = (D_o - D_i)/\ln(D_o/D_i)$ for a symmetric fiber. For an asymmetric fiber, πD_o is to be used for membrane surface area per unit length with δ being the membrane thickness.

All these assumptions were utilized by Pan and Habgood (1978) except assumption 7. In addition, instead of assumption 6, they assumed the permeate viscosity to vary linearly with the permeate mole fraction. The effects of these two additional assumptions are expected to be of a minor nature. We note in passing that the Pan and Habgood (1978) analysis for an asymmetric fiber based on assumption 8 does ignore the cross-flow effect that exists within the porous substrate of an asymmetric fiber (Pan, 1983).

Following Pan and Habgood (1978) with the only difference that species 1 is the more permeable component and species 2 is the less permeable, we can obtain the following dimensionless equations for the *cocurrent hollow fiber permeator* (Figure 1a):

$$\frac{dx}{dR_f} = \left(\frac{y-x}{x_f-y}\right)\{\alpha(1-x)(x-\gamma y) - x[(1-x)-\gamma(1-y)]\} \quad (1)$$

$$\frac{dy}{dR_f} = \left(\frac{y-x}{x_f-x}\right)\{\alpha(1-y)(x-\gamma y) - y[(1-x)-\gamma(1-y)]\} \quad (2)$$

$$\frac{d\gamma^2}{dR_f} = -\left\{\frac{256\mu RTL_f^2}{\pi^2\left(\frac{Q_2}{\delta}\right)D_{lm}D_i^4P_f^3}\right\}\left(\frac{x_f-x}{y-x}\right) = -\beta\left(\frac{x_f-x}{y-x}\right) \quad (3)$$

The first two equations are identical with those in Boucif et al. (1984), while the last one not used by them expresses the gas pressure drop inside the rigid hollow fiber. If one has an asymmetric fiber, replace D_{lm} in eq 3 by D_o, the outside hollow fiber diameter. The relevant dimensionless quantities in the above equations are defined by

$$\gamma = p/P_f; \quad \alpha = Q_1/Q_2 \quad (4)$$

$$R_f = \left(\frac{Q_2}{\delta}\right)\frac{P_f\pi D_{lm}l}{L_f} \quad (4a)$$

$$R_{fT} = \left(\frac{Q_2}{\delta}\right)\frac{P_f\pi D_{lm}l_w}{L_f} \quad (4b)$$

$$\beta = \frac{256\mu RTL_f^2}{\left(\frac{Q_2}{\delta}\right)\pi^2D_{lm}D_i^4P_f^3} \quad (4c)$$

where the pressure ratio γ (≤ 1) varies along the membrane length due to a variation in p. Further, R_f is the nondimensional area for cocurrent flow measured with the origin at high-pressure feed entry point up to any location of active fiber length l (Figure 1a). If the total active length of the fiber is l_w, the corresponding nondimensional membrane area is R_{fT} for cocurrent flow. The initial and boundary conditions for the three governing equations are

$$\text{at } l = 0: \quad R_f = 0, x = x_f, y = y_f, \gamma = \gamma_f, V = 0 \quad (5)$$

$$\text{at } l = l_w: \quad R_f = R_{fT}, \gamma = \gamma_w, x = x_w, V = V_w, y = y_w \quad (6)$$

Note $y = y_f$ and $\gamma = \gamma_f$ are not specified in the problem. Usually $x = x_f$ and $\gamma = \gamma_w$ are known. If the problem involves designing a permeator, then one of the stream conditions at the reject end, say, $x = x_w$ (or $y = y_w$), will be specified with R_{fT} to be determined. For rating problems, the total membrane area and therefore R_{fT} is known with the reject and permeate stream conditions to be determined.

To complete the cocurrent flow problem statement, we indicate below the overall and more permeable component mass balances over an envelope extending from the feed

end to any arbitrary location where the hollow fiber length is l:

$$L_f = V + L \tag{7}$$

$$L_f x_f = Vy + Lx \tag{8}$$

The cut θ for the cocurrent permeator is defined as

$$\theta = \frac{V_w}{L_f} = \frac{L_f - L_w}{L_f} \tag{9}$$

Using eq 8 for the whole permeator, one obtains

$$x_f = \theta y_w + (1 - \theta)x_w \tag{10}$$

from which the cut θ is obtained as

$$\theta = \frac{x_f - x_w}{y_w - x_w} \tag{11}$$

For the countercurrent flow hollow fiber permeator (Figure 1b), the nondimensionalized governing equations corresponding to eq 1–3 may be written as

$$\frac{dx}{dR_w} = \left(\frac{y - x}{y - x_w}\right)\{\alpha(1 - x)(x - \gamma y) - x[(1 - x) - \gamma(1 - y)]\} \tag{12}$$

$$\frac{dy}{dR_w} = \left(\frac{y - x}{x - x_w}\right)\{\alpha(1 - y)(x - \gamma y) - y[(1 - x) - \gamma(1 - y)]\} \tag{13}$$

$$\frac{d\gamma^2}{dR_w} = -\left\{\frac{256\mu RTL_f^2}{\pi^2(Q_2/\delta)D_{lm}D_i^4P_f^3}\right\}\left(\frac{x - x_w}{y - x}\right)\left(\frac{L_w}{L_f}\right)^2 = -\beta\left(\frac{x - x_w}{y - x}\right)\left(\frac{x_f - y_f}{x_w - y_f}\right)^2 \tag{14}$$

with the nondimensional membrane area R_w being based on the fiber length l increasing from the high-pressure reject end and the molar high-pressure reject flow L_w:

$$R_w = \left(\frac{Q_2}{\delta}\right)\frac{P_f\pi D_{lm}l}{L_w} = R_f^{cc}\left(\frac{L_f}{L_w}\right) \tag{15}$$

The quantity β is defined as before by eq 4c. For a total fiber length of l_w, the nondimensional membrane area is R_{wT} where

$$R_{wT} = \left(\frac{Q_2}{\delta}\right)\frac{P_f\pi D_{lm}l_w}{L_w} = R_{fT}^{cc}\left(\frac{L_f}{L_w}\right) \tag{16}$$

Since only one fiber has been shown in Figure 1a,b, the flow rates L_f, L_w, V_w, and V_f are on a single fiber basis. For the usual multifiber information, single fiber flow rates are obtained simply by dividing it by the number of fibers.

The three governing equations (12) to (14) are to be solved by using the following conditions: (i) At high-pressure feed inlet

$$R_w = R_{wT}, \quad l = l_w, \quad x = x_f, \quad L = L_f, \; V = V_f, \quad y = y_f, \quad \gamma = \gamma_f \tag{17}$$

(ii) At high-pressure reject stream location

$$R_w = 0, \quad l = 0, \quad x = x_w, \quad L = L_w, \quad V = 0, \; y = y_w, \quad \gamma = \gamma_w \tag{18}$$

Note that $y = y_w$ and $\gamma = \gamma_w$ are not specified in the problem. But $x = x_f$, $L = L_f$, and $\gamma = \gamma_f$ are known. For a permeator design problem, one of the product stream conditions, say, $x = x_w$ (or $y = y_f$), will be specified with R_{wT} (and therefore l_w) to be determined. For rating problems, the total membrane length l_w is known and reject and permeate stream conditions are to be determined.

The countercurrent flow problem statement is completed by including the overall and more permeable component mass balances over an envelope extending from the high-pressure reject end to any point at a distance l from the latter end:

$$L = L_w + V \tag{19}$$

$$Lx = L_w x_w + Vy \tag{20}$$

The cut θ for the countercurrent permeator is defined as

$$\theta = \frac{V_f}{L_f} = \frac{L_f - L_w}{L_f} \tag{21}$$

The relation corresponding to eq 10 is

$$x_f = \theta y_f + (1 - \theta)x_w \tag{22}$$

from which

$$\theta = \frac{x_f - x_w}{y_f - x_w} \tag{23}$$

A Series Solution for Cocurrent Flow Hollow Fiber Permeator

To solve eq 1–3, subject to initial condition 5 and the condition $\gamma = \gamma_w$ at $R_f = R_{fT}$ of condition 6, we assume the following series solutions for x, y, and γ in terms of R_f:

$$x = a_0 + a_1R_f + a_2R_f^2 + a_3R_f^3 + \ldots \tag{24}$$

$$y = b_0 + b_1R_f + b_2R_f^2 + b_3R_f^3 + \ldots \tag{25}$$

$$\gamma = c_0 + c_1R_f + c_2R_f^2 + c_3R_f^3 + \ldots \tag{26}$$

The infinite series for each of x, y, and γ will be truncated here after the R_f^3 term. Substitute these expressions into eq 1–3 and collect terms of order R_f^0, R_f^1, R_f^2, and R_f^3. These lead to a total of 12 algebraic equations for the 12 unknowns a_0, b_0, c_0, a_1, b_1, c_1, a_2, b_2, c_2, a_3, b_3, and c_3. Imposing the initial conditions 5, i.e., $R_f = 0$, $x = x_f$, onto eq 24 yields

$$a_0 = x_f \tag{27}$$

Further, at $R_f = 0$, $\gamma = \gamma_f$ (which is unknown) leads to

$$c_0 = \gamma_f \tag{28}$$

from eq 26.

We use these two results now in 2 of the 12 algebraic equations relating a_0, b_0, c_0, a_1, and b_1. Fortunately, the coefficient of b_1 is $x_f - a_0$, i.e., 0, so that we have two simple algebraic equations for a_1 and b_0 to be expressed in terms of a_0 (= x_f) and c_0 (= γ_f). The equation for b_0 is a cubic

$$(b_0 - x_f) \times \{\alpha x_f - b_0 + (1 - \alpha)x_f b_0 + (1 - \alpha)b_0\gamma_f + (\alpha - 1)b_0^2\gamma_f\} = 0 \tag{29}$$

Since b_0 is obviously greater than x_f, we find

$$\{\alpha x_f - b_0 + (1 - \alpha)x_f b_0 + (1 - \alpha)b_0\gamma_f + (\alpha - 1)b_0^2\gamma_f\} = 0 \tag{30}$$

from which the negative root (being the physically meaningful one) is

$$b_0 = ([1 - (1 - \alpha)(x_f + \gamma_f)] - \{[(1 - \alpha) \times (x_f + \gamma_f) - 1]^2 - 4(\alpha - 1)\alpha x_f\gamma_f\}^{1/2})/[2(\alpha - 1)\gamma_f] \tag{31}$$

Correspondingly

$$a_1 = -\{(\alpha - 1)x_f + (1 - \alpha)x_f^2 + x_f\gamma_f - \alpha b_0\gamma_f + (\alpha - 1)x_f b_0\gamma_f\} \quad (32)$$

Note here that b_0, given by eq 31, is y_f for cocurrent flow. It depends on γ_f which is an unknown at this stage but will be known after the whole procedure is carried out. Thus, a_1 and b_0 depend on α, x_f, and γ_f.

When the remaining algebraic equations are solved, the following expressions for c_1, b_1, a_2, b_2, c_2, a_3, b_3, and c_3 are obtained:

$$c_1 = 0 \quad (33)$$

$$b_1 = \frac{(b_0 - x_f)\{\alpha a_1 + (1 - \alpha)a_1 b_0\}}{(b_0 - x_f)\{1 - (1 - \alpha)(x_f + \gamma_f - 2b_0\gamma_f)\} - a_1} \quad (34)$$

$$a_2 = -\tfrac{1}{2}\{(\alpha - 1)a_1 + 2(1 - \alpha)x_f a_1 + \gamma_f(a_1 - \alpha b_1) + (\alpha - 1)(a_1 b_0 + x_f b_1)\gamma_f\} + a_1^2/[2(x_f - b_0)] \quad (35)$$

$$b_2 = [(b_0 - x_f)a_2 b_1 + (b_0 - x_f)^2\{\alpha a_2 + (1 - \alpha) \times (a_2 b_0 + a_1 b_1 + b_0 c_2 - b_1^2\gamma_f - b_0^2 c_2)\} - (b_1 - a_1)a_1 b_1]/[(b_0 - x_f)^2\{1 - (1 - \alpha)(\gamma_f + x_f - 2b_0\gamma_f)\} - 2a_1(b_0 - x_f)] \quad (36)$$

$$c_2 = -\frac{a_1\beta}{4\gamma_f(x_f - b_0)} \quad (37)$$

$$a_3 = -\frac{1}{3}\{(\alpha - 1)a_2 + (1 - \alpha)(a_1^2 + 2x_f a_2) + (a_2\gamma_f + x_f c_2) - \alpha(b_2\gamma_f + b_0 c_2) + (\alpha - 1)[\gamma_f(a_2 b_0 + a_1 b_1 + x_f b_2) + x_f b_0 c_2]\} + \frac{a_2 a_1}{x_f - b_0} + \frac{(b_1 - a_1)a_1^2}{3(x_f - b_0)^2} \quad (38)$$

$$b_3 = [(b_0 - x_f)^3\{\alpha a_3 + (1 - \alpha)(a_3 b_0 + a_2 b_1 + a_1 b_2 + b_1 c_2 + b_0 c_3 - 2b_1 b_2\gamma_f - 2b_0 b_1 c_2 - b_0^2 c_3)\} + (2a_2 b_2 + a_3 b_1)(b_0 - x_f)^2 + (b_1 - a_1)^2 a_1 b_1 - [(2a_1 b_2 + a_2 b_1)(b_1 - a_1) + (b_2 - a_2)a_1 b_1](b_0 - x_f)]/((b_0 - x_f)^2[(b_0 - x_f)\{1 - (1 - \alpha)(x_f + \gamma_f - 2b_0\gamma_f)\} - 3a_1]) \quad (39)$$

$$c_3 = -\frac{a_2\beta + 4\gamma_f c_2(a_1 - b_1)}{6\gamma_f(x_f - b_0)} \quad (39a)$$

All the 12 coefficients in truncated series expansions 24–26 are now explicitly available in terms of x_f, α, and γ_f, among which γ_f is still unknown. For $R_f = R_{fT}$ corresponding to reject end location, truncated expansions 24, 25, and 26 yield respectively from condition 6

$$x_w = x_f + a_1(x_f,\alpha,\gamma_f)R_{fT} + a_2(x_f,\alpha,\gamma_f)R_{fT}^2 + a_3(x_f,\alpha,\gamma_f)R_{fT}^3 \quad (40)$$

$$y_w = b_0(x_f,\alpha,\gamma_f) + b_1(x_f,\alpha,\gamma_f)R_{fT} + b_2(x_f,\alpha,\gamma_f)R_{fT}^2 + b_3(x_f,\alpha,\gamma_f)R_{fT}^3 \quad (41)$$

$$\gamma_w = \gamma_f + c_2(x_f,\alpha,\gamma_f)R_{fT}^2 + c_3(x_f,\alpha,\gamma_f)R_{fT}^3 \quad (42)$$

If now R_{fT} or l_w is specified for a *rating problem*, solve the algebraic eq 42 numerically for the unknown γ_f for known x_f, α, and γ_w. Substitute this value of γ_f in eq 40 and 41 to determine x_w and y_w. On the other hand, for a *design problem*, if, say, x_w is specified (with x_f, α, and γ_w being known), then solve eq 40 and 42 simultaneously for two unknowns, γ_f and R_{fT}. The value of y_w is obtained from eq 41 by just substituting the values of γ_f and R_{fT} determined above. Knowledge of x_w and y_w, for example, allows calculation of θ from eq 11. Similarly, other mass balance relations may be used for determining flow rates of product and reject streams. With a design problem where y_w is specified, solve eq 41 and 42 for unknowns γ_f and R_{fT}.

A Series Solution for Countercurrent Flow Hollow Fiber Permeator

To solve eq 12–14 subject to the specified conditions, we assume the following series solutions for x, y, and γ in terms of R_w:

$$x = d_0 + d_1 R_w + d_2 R_w^2 + d_3 R_w^3 + \ldots \quad (43)$$

$$y = e_0 + e_1 R_w + e_2 R_w^2 + e_3 R_w^3 + \ldots \quad (44)$$

$$\gamma = f_0 + f_1 R_w + f_2 R_w^2 + f_3 R_w^3 + \ldots \quad (45)$$

Each infinite series is truncated after the R_w^3 term. The truncated expansions are substituted for x, y, and γ in eq 12, 13, and 14, and terms of order R_w^0, R_w^1, R_w^2, and R_w^3 are collected. Twelve algebraic equations in terms of 12 unknown coefficients, d_0, d_1, d_2, d_3, e_0, e_1, e_2, e_3, f_0, f_1, f_2, and f_3, are obtained. Using condition 18 at high-pressure reject end as $x = x_w$ and $\gamma = \gamma_w$ for $R_w = 0$, we get

$$d_0 = x_w \quad (46)$$

$$f_0 = \gamma_w \quad (47)$$

Using these results in eq 13 and 14 containing unknowns d_1 and e_0, we obtain

$$d_1 = (\alpha - 1)x_w + (1 - \alpha)x_w^2 + x_w\gamma_w - \alpha e_0\gamma_w + (\alpha - 1)x_w e_0\gamma_w \quad (48)$$

and

$$e_0 = ([1 - (1 - \alpha)(x_w + \gamma_w)] - \{[(1 - \alpha) \times (x_w + \gamma_w) - 1]^2 - 4(\alpha - 1)\alpha x_w\gamma_w\}^{1/2})/[2(\alpha - 1)\gamma_w] \quad (49)$$

$$e_0 = y_w \quad (49a)$$

In obtaining the last result, we rejected the physically meaningless solution of $e_0 = x_w$. Further, in the resulting quadratic, the negative root, being the physically meaningful one, was accepted. This quantity e_0 represents the value of y at the high-pressure reject stream end where γ_w is specified i.e., y_w.

At this time note that y_f may be represented as a result of eq 49a as

$$y_f = y_w + e_1 R_{wT} + e_2 R_{wT}^2 + e_3 R_{wT}^3 \quad (49b)$$

For a permeator with given feed conditions and exit pressure ratio, γ_f, define

$$x_w - y_w - e_1 R_{wT} - e_2 R_{wT}^2 - e_3 R_{wT}^3 = A \quad (49c)$$

and

$$x_f - y_w - e_1 R_{wT} - e_2 R_{wT}^2 - e_3 R_{wT}^3 = B \quad (49d)$$

By solving the remaining algebraic equations, we obtain the following explicit expressions for the remaining coefficients in the series expansions 43, 44, and 45:

$$f_1 = 0 \quad (50)$$

$$e_1 = \frac{(e_0 - x_w)[\alpha d_1 + (1 - \alpha)d_1 e_0]}{d_1 + (e_0 - x_w)[1 - (1 - \alpha)(x_w + \gamma_w - 2e_0\gamma_w)]} \quad (51)$$

$$d_2 = \tfrac{1}{2}[(\alpha - 1)d_1 + 2(1 - \alpha)x_w d_1 + d_1\gamma_w - 2e_1\gamma_w + (\alpha - 1)(d_1 e_0 + x_w e_1)\gamma_w] - d_1^2/[2(e_0 - x_w)] \quad (52)$$

$$f_2 = \frac{d_1\beta B^2}{4A^2\gamma_w(x_w - e_0)^3} \quad (53)$$

$$e_2 = \{(e_0 - x_w)^2[\alpha d_2 + (1-\alpha)(d_2e_0 + d_1e_1 + e_0f_2 - e_1^2\gamma_w - e_0^2f_2)] - e_1d_2(e_0 - x_w) + (e_1 - d_1)e_1d_1\}/[(e_0 - x_w)\{2d_1 + (e_0 - x_w)[1 - (1-\alpha)(x_w + \gamma_w - 2e_0\gamma_w)]\}] \quad (54)$$

$$f_3 = \frac{-4f_0f_2(e_1 - d_1)A^2 - B^2d_2\beta}{6A^2\gamma_w(x_w - e_0)^3} \quad (55)$$

$$d_3 = \frac{1}{3}[(\alpha-1)d_2 + (1-\alpha)(d_1^2 + 2x_wd_2) + (d_2\gamma_w + x_wf_2) - \alpha(e_2\gamma_w + e_0f_2) + (\alpha-1)\{\gamma_w(d_2e_0 + d_1e_1 + x_we_2) + x_we_0f_2\}] + \frac{d_1^2(e_1 - d_1) - 3d_1d_2}{3(e_0 - x_w)} \quad (56)$$

$$e_3 = \{(e_0 - x_w)^3[\alpha d_3 + (1-\alpha)(d_3e_0 + d_2e_1 + d_1e_2 + e_1\gamma_w + e_0f_3 - 2e_1e_2\gamma_w - 2e_0e_1f_2 - e_0^2f_3)] - (2e_2d_2 + e_1d_3)(e_0 - \gamma_w)^2 + [(e_1 - d_1)(2e_2d_1 + e_1d_2) + (e_2 - d_2)e_1d_1](e_0 - x_w) - e_1d_1(e_1 - d_1)^2\}/\{(e_0 - x_w)^2[3d_1 - (e_0 - d_0)\{(1-\alpha)(d_0 + \gamma_w - 2e_0\gamma_w) - 1\}]\} \quad (57)$$

Thus, the 12 coefficients in expansions 43, 44, and 45 are expressed explicitly in terms of x_f, α, x_w, γ_w, and R_{wT}. From definition 16, R_{wT} may be expressed

$$R_{wT} = \left(\frac{Q_2}{\delta}\right)\frac{P_f\pi D_{lm}l_w}{L_f}\left(\frac{y_f - x_w}{y_f - x_f}\right) \quad (58)$$

For a rating problem with l_w known, R_{wT} is then a function of y_f and x_w. For a design problem with y_f specified, R_{wT} is a simple function of l_w and x_w. For a design problem with x_w specified, R_{wT} is a function of l_w and y_f. With that perspective, at $R_w = R_{wT}$, corresponding to feed end location, conditions 17 applied to truncated expansions 43, 44, and 45 yield respectively

$$x_f = x_w + d_1(\alpha,x_f,x_w,\gamma_w)R_{wT} + d_2(\alpha,x_f,x_w,\gamma_w)R_{wT}^2 + d_3(\alpha,x_f,x_w,\gamma_w,R_{wT})R_{wT}^3 \quad (59)$$

$$y_f = y_w(\alpha,x_f,x_w,\gamma_w) + e_1(\alpha,x_f,x_w,\gamma_w)R_{wT} + e_2(\alpha,x_f,x_w,\gamma_w)R_{wT}^2 + e_3(\alpha,x_f,x_w,\gamma_w,R_{wT})R_{wT}^3 \quad (60)$$

$$\gamma_f = \gamma_w + f_2(\alpha,x_f,x_w,\gamma_w,R_{wT})R_{wT}^2 + f_3(\alpha,x_f,x_w,\gamma_w,R_{wT})R_{wT}^3 \quad (61)$$

Consider *permeator design problems* now. Suppose x_w is specified for known x_f, α, and γ_f. Then in eq 59 and 61, there are two unknowns, γ_w and R_{wT}. Solve these two algebraic equations simultaneously and numerically for γ_w and R_{wT}. Substitute these values in eq 60 to determine y_f. The value of l_w is next obtained when y_f and x_w are substituted in eq 58. Obtain θ now from eq 23 and L_w from eq 21.

If in a *permeator design problem* y_f is specified for known x_f, α, and γ_f, the unknowns are x_w, γ_w, and R_{wT}. Note here that from eq 49c and 49d

$$A = x_w - y_f \quad \text{and} \quad B = x_f - y_f \quad (61a)$$

Therefore, the coefficients d_3 and e_3 (which have R_{wT} dependence due to their dependence on f_2 and f_3 which in turn depend on R_{wT} due to eq 49c and 49d) depend simply on x_w and known y_f. Further, f_2 and f_3 do not depend on R_{wT}; instead they depend on x_w and known y_f. Thus, there are three algebraic equations, eq 59, 60, and 61, with three unknowns, x_w, γ_w, and R_{wT}, with R_{wT} never appearing with a power greater than 3. Solve these three simultaneously to obtain x_w, γ_w, and R_{wT}. From eq 58, l_w is known for the value of R_{wT} obtained. The rest of the procedure is straightforward.

For a *rating problem*, l_w or membrane area is specified. With R_{wT} given by eq 58, we see that R_{wT} may be replaced in terms of unknowns y_f and x_w. Further, with A and B expressed by eq 61a, we have three algebraic equations, eq 59, 60, and 61, for three unknowns, x_w, y_f, and γ_w. These are to be solved simultaneously in a computer to yield values of x_w, y_f, and γ_w. Although the countercurrent permeator problem based on series solutions is numerically more demanding, it is far simpler than solving a boundary value problem with three coupled differential equations and guessing the conditions at the reject end with backward integrations.

Numerical Solutions for Countercurrent and Cocurrent Hollow Fiber Permeators

It is necessary to recognize first that since there is a pressure drop inside the fiber luman and since the permeate pressure can be specified only at the exit end of the fiber, both cocurrent and countercurrent flow patterns become boundary value problems here. This situation is unlike that considered in Boucif et al. (1984), where the no pressure drop cocurrent permeator was an initial value problem.

For either flow pattern, before one can solve the system of differential equations, one needs to know the value of y at the closed end of the fiber. This is done by using the cross-flow criterion at that point (Pan and Habgood, 1978). For cocurrent flow, it means that, at $l = 0$, $y = y_f$ is obtained from

$$y_f/(1 - y_f) = \{\alpha(x_f - \gamma_fy_f)\}/\{1 - x_f - \gamma_f(1 - y_f)\} \quad (62)$$

One has to select the right root in the above quadratic. The value of dy/dR_f at the closed end of the fiber is indeterminate and the L'Hospital rule has to be used. For cocurrent flow, we have

$$\left.\frac{dy}{dR_f}\right|_{l=0} = \frac{\{\alpha - y_f(\alpha-1)\}\frac{dx}{dR_f} - (\alpha-1)y_f(1-y_f)\frac{d\gamma}{dR_f}}{2 + 2(\alpha-1)x_f + (\alpha-2)\gamma_f - 3(\alpha-1)\gamma_fy_f} \quad \text{at } R_f = 0 \quad (63)$$

For countercurrent flow, equations similar to (62) and (63) have to be used to obtain the value of y at $l = 0$, i.e., y_w and its derivative with respect to nondimensional area. However, replace y_f by y_w, γ_f by γ_w, and x_f by x_w.

For actual numerical solution, the countercurrent problem, as defined by eq 12–14, was reformulated in a different way with R_f^{cc} as the independent variable instead of R_w. This was done because L_w, needed to compute R_{wT}, is not known a priori. At this time, it is advantageous to incorporate V and L as two extra variables in the set of ordinary differential equations:

$$\frac{dV}{dR_f^{cc}} = L_f[\alpha(x - \gamma y) + 1 - x - \gamma(1 - y)] \quad (64)$$

$$dL/dR_f^{cc} = dV/dR_f^{cc} \quad (64a)$$

The associated boundary conditions are

$$\text{at } R_f^{cc} = 0, \quad V = 0 \quad (64b)$$

$$\text{at } R_f^{cc} = R_{fT}^{cc}, \quad L = L_f \quad (64c)$$

This formulation is similar to that adopted by Sengupta and Sirkar (1984).

For solving the boundary value problems of cocurrent or countercurrent flow, an available packaged software

(IMSL subrouting DVCPR) was used. The routine is based on the PASVA3 program (Pereyra, 1978) with adaptive finite difference approach. To use this routine, it is usually necessary to supply initial estimates of the values of each of the variables at user-selected grid points across the domain, including the boundaries. The initial estimates can be generated in the present case by solving the same problem once with artificially simplified boundary conditions. One can first solve the cocurrent no pressure drop problem, for example, by assuming that γ_f is the same as γ_w (which is known for cocurrent problem) and calculating y_f from eq 62. Since there is no pressure drop, one needs to solve now only eq 1 and 2 from $R_f = 0$ to $R_f = R_{fT}$. This initial value problem can be solved by using, e.g., a fourth-order Runge–Kutta method. The values of each variable at user-selected grid points across the domain are stored in the computer memory. These are used as the starting values by the routine DVCPR. To operate the routine, the user needs to supply the derivatives, the boundary conditions, and the Jacobian matrix for the actual system of differential equations. The subroutine initiates a series of iterations which gradually improve the values of the variables until the actual set of differential equations and boundary conditions are simultaneously satisfied. The solution technique is same for countercurrent flow.

For the numerical calculations, two sets of parameters have been used as far as feed pressure, feed flow rate, and permeability of the less permeating component are concerned. For both sets of parameters, however, the temperature, viscosity, and fiber dimensions have the same values. They are as follows: $T = 25\ °C = 298\ K$; $\mu = 0.015$ cP $= 1.5 \times 10^{-5}$ Pa s; $D_i = 150\ \mu m = 1.5 \times 10^{-4}$ m; $D_o = 300\ \mu m = 3.0 \times 10^{-4}$ m; $D_{lm} = (D_o - D_i)/\ln(D_o/D_i) = 2.164 \times 10^{-4}$ m.

Calculations have been carried out for $\alpha = 5$, 10, 25, 30, and 80. For $\alpha = 5$ or 10, the following values of P_f, L_f, and Q_2/δ were used: $P_f = 25$ atm; $L_f = 65$ cm^3 (STP)/min $= 4.491 \times 10^{-5}$ mol/s; $Q_2/\delta = 8.8 \times 10^{-6}$ cm^3 (STP)/(s cm^2 cmHg) $= 2.7362 \times 10^{-9}$ mol/(s m^2 Pa).

For values of α of 25, 30, or 80, the following corresponding values were used: $P_f = 40$ atm; $L_f = 60$ cm^3 (STP)/min $= 4.145 \times 10^{-5}$ mol/s; $Q_2/\delta = 1.82 \times 10^{-6}$ cm^3 (STP)/(s cm^2 cmHg) $= 5.659 \times 10^{-10}$ mol/(s m^2 Pa).

Calculations have also used three different exit values of γ, 0.1, 0.25, and 0.05, and three different values of x_f, 0.209, 0.05, and 0.50. Only a single fiber has been used in the calculation under conditions such that a very significant pressure drop takes place in the hollow fiber bore. Multifiber calculations can be easily adapted to the present arrangement simply by obtaining the feed flow rate per fiber which is L_f in our calculations. This is possible since shell side flow effects and pressure drops (if any) are of no importance to the problem. Further, for membrane area specification, fiber number and length are independent quantities with the length to be determined, usually for given fiber numbers.

The numerical solution of algebraic equations obtained from the series solutions are obtained by using a simple Newton–Raphson technique. The IMSL subroutine ZSPOW was used for solving either one algebraic equation containing one unknown or simultaneously two algebraic equations containing two unknowns. The CPU time required for these calculations was, in general, 8–9 times smaller than the corresponding time required for numerical solutions. For the purpose of comparing cocurrent and countercurrent permeators with given α, x_f, and exit values of γ and β, countercurrent permeator results from series solution are expressed in terms of R_{fT}^{cc} instead of R_{wT} with l, however, starting from the high-pressure reject end. Since cocurrent results are expressed against R_{fT}, both flow patterns can be compared on an equivalent basis for equal l_w and L_f.

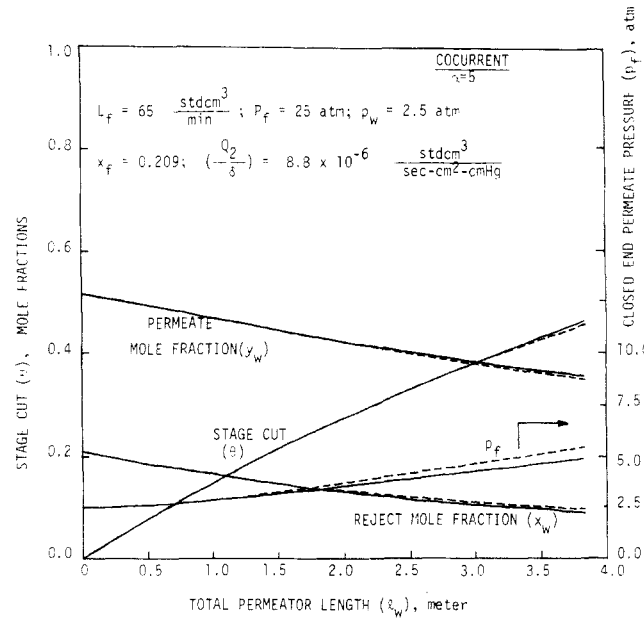

Figure 2. Comparison of series and numerical solutions for cocurrent hollow fiber permeators for $x_f = 0.209$, $\alpha = 5$, $\gamma_w = 0.1$, $P_f = 25$ atm, $L_f = 65$ cm^3 (STP)/min, and $Q_2/\delta = 8.8 \times 10^{-6}$ cm^3 (STP)/(s cm^2 cmHg).

Comparisons of Series Solutions with Numerical Solutions

Cocurrent Hollow Fiber Gas Permeators. We present below the results of calculations in terms of values of exit compositions, closed-end permeate pressures, and stage cuts plotted against l_w, the totel permeator length, for different cocurrent hollow fiber gas permeators. Two types of results are plotted in each figure. The solid lines represent the results obtained by using the series solutions developed here. The dashed lines display the numerical solutions for the same parametric conditions. The juxtaposition of the numerical results on the series solutions will identify the ranges of validity of the series solutions. It is useful to recall here that the usual ranges of cut θ encountered in commercial permeators vary from around 0 to about 0.45–0.5. Thus, we will not be concerned with the accuracy of the series solution predictions for high values of cut.

Figure 2 compares the cocurrent series solution predictions of y_w, x_w, p_f, and θ against l_w with a numerical solution for $x_f = 0.209$, $\alpha = 5$, $p_w = 2.5$ atm, and $Q_2/\delta = 8.8 \times 10^{-6}$. Each value of l_w represents a different permeator for given operating conditions. The conditions are such that, at the highest membrane length used ($l_w = 3.8$ m), the value of cut θ is almost 0.5. Further, there is a significant pressure drop such that, for a permeator of $l_w = 3.8$m, p_f is around 5 atm with $p_w = 2.5$ atm. Note that, unlike in Boucif et al. (1984), the curves of y_w and x_w against l_w cannot be used to indicate the composition profiles along a cocurrent permeator. Further, the value of p_f for any permeator with a given l_w is only indicated in Figure 2. Thus, p_f values, as shown, apparently rise with l_w, whereas an actual p profile decreases along the length of a cocurrent permeator from a high value of p_f to p_w.

It is clear from Figure 2 that, for the low value of $\alpha = 5$, the predictive accuracy of the series solutions for y_w, x_w,

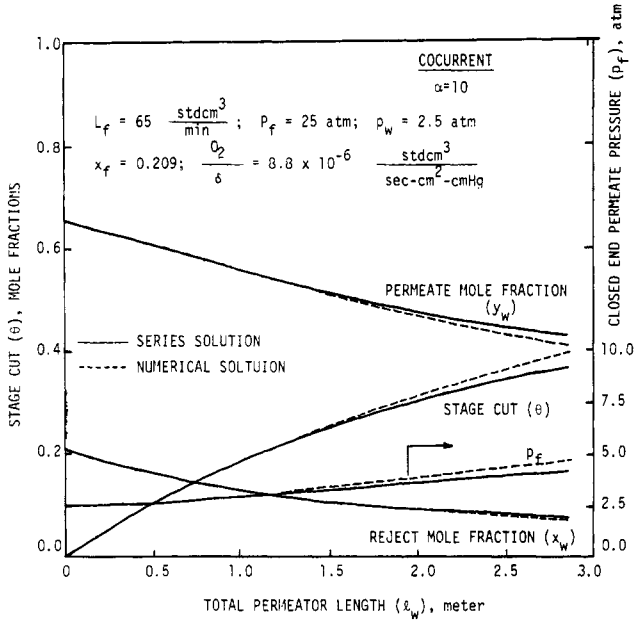

Figure 3. Comparison of series and numerical solutions for cocurrent hollow fiber permeators for $x_f = 0.209$, $\alpha = 10$, $\gamma_w = 0.1$, and other parameters same as in Figure 2.

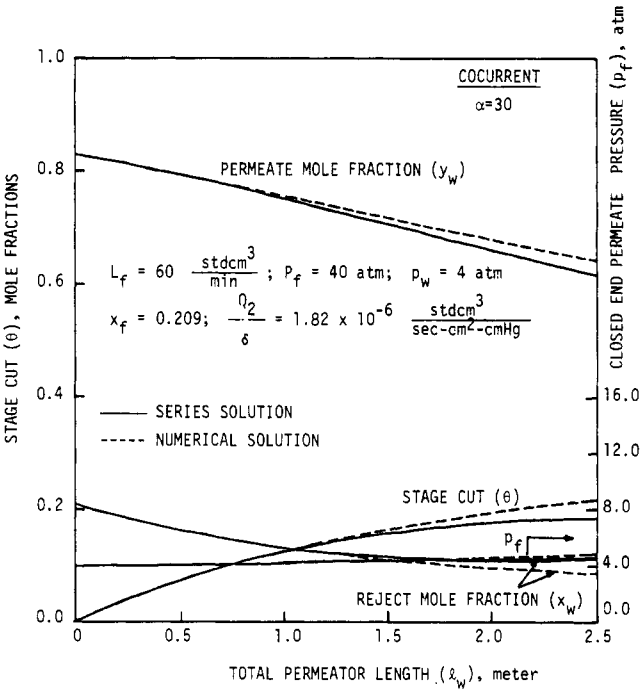

Figure 4. Comparison of series and numerical solutions for cocurrent hollow fiber permeators for $x_f = 0.209$, $\alpha = 30$, $\gamma_w = 0.1$, $P_f = 40$ atm, $L_f = 60$ cm³ (STP)/min, and $Q_2/\delta = 1.82 \times 10^{-6}$ cm³ (STP)/(s cm² cmHg).

and θ is very high, even at the highest cut level used. The accuracy in p_f prediction at the highest θ values is slightly lower. However, the effect of this deviation in p_f values is highly attenuated insofar as predictions of y_w, x_w, and θ are concerned. Since for design or rating purposes one is interested only in y_w, x_w, and θ for a particular l_w, we conclude that the series solutions are highly efficient for $\alpha = 5$.

Figure 3 explores the comparative behavior when α is increased to 10 while all other conditions are exactly those used in Figure 2. The accuracy of x_w predictions appears to be very high. At the highest l_w (= 2.8 m) corresponding to a cut of 0.40, the error in predicting y_w is less than 6% while that in predicting θ is around 8%. The error in

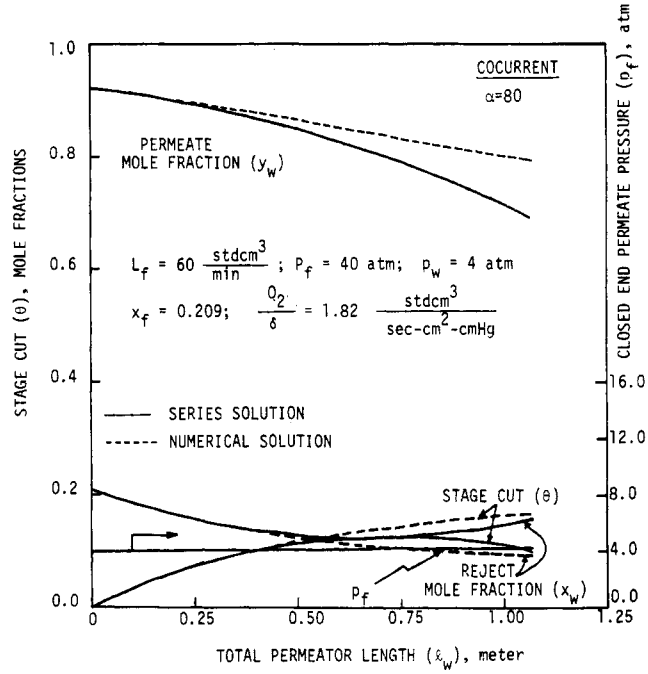

Figure 5. Comparison of series and numerical solutions for cocurrent hollow fiber permeators for $x_f = 0.209$, $\alpha = 80$, $\gamma_w = 0.1$, and other parameters same as in Figure 4.

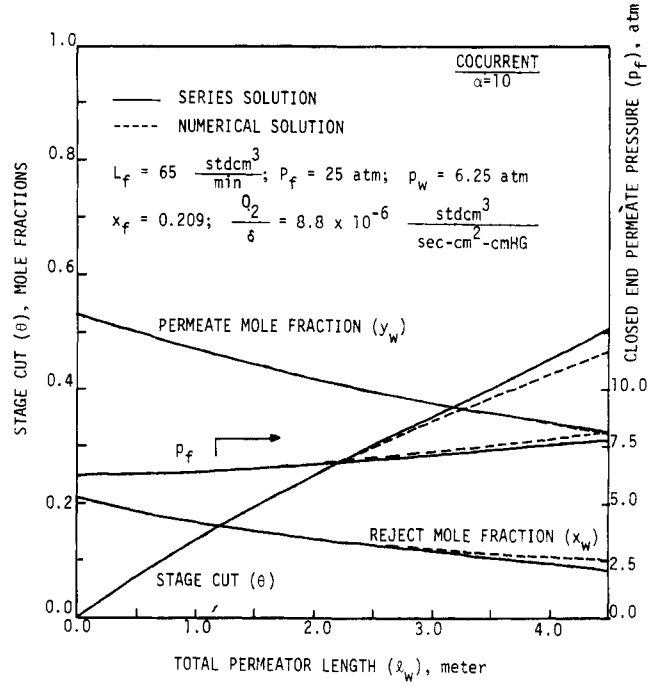

Figure 6. Comparison of series and numerical solutions for cocurrent hollow fiber permeators for $x_f = 0.209$, $\alpha = 10$, $\gamma_w = 0.25$, and other parameters same as in Figure 2.

predicting p_f is similar to that in Figure 2.

When α is increased to 30, the comparative behavior shown in Figure 4 indicates that the series solutions are quite accurate up to a $\theta \simeq 0.20$ beyond which errors in θ and x_w predictions become considerable. Figure 5, calculated for $\alpha = 80$, similarly illustrates that, beyond a cut of $\theta \simeq 0.14$, considerable errors are encountered if series solutions are used. The behavior is similar to that observed by Boucif et al. (1984). Note that the values of L_f, P_f, p_w, and Q_2/δ in Figures 4 and 5 are different from those in Figures 2 and 3.

The cases considered so far utilized $\gamma_w = 0.10$. Figure 6 explores the results for a higher $\gamma_w = 0.25$ at $\alpha = 10$, $x_f = 0.209$, $P_f = 25$ atm, and $p_w = 6.25$ atm. Other conditions

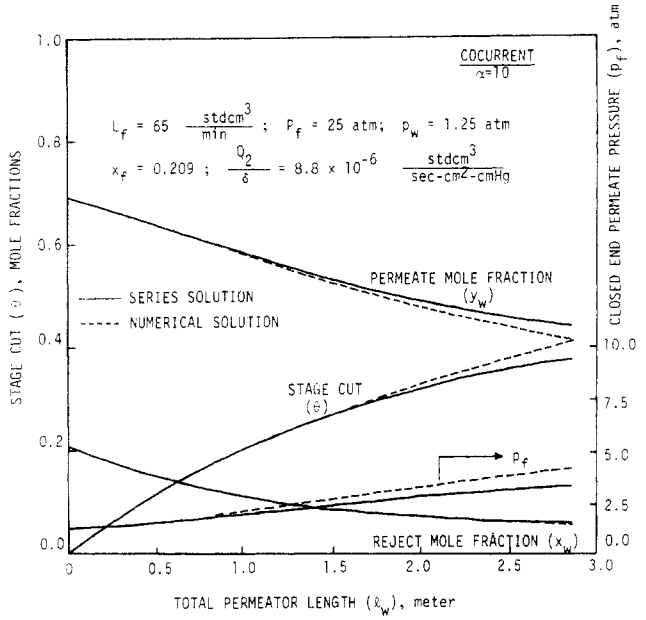

Figure 7. Comparison of series and numerical solutions for cocurrent hollow fiber permeators for $x_f = 0.209$, $\alpha = 10$, $\gamma_w = 0.05$, and other parameters same as in Figure 2.

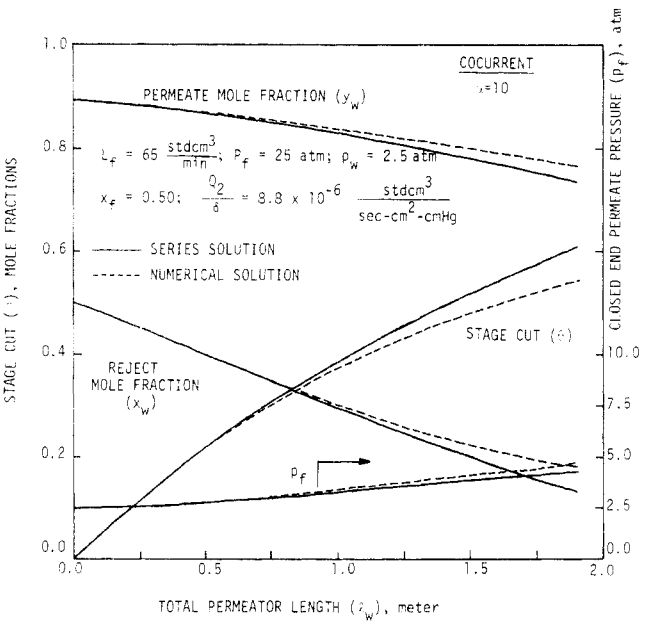

Figure 8. Comparison of series and numerical solutions for cocurrent hollow fiber permeators for $x_f = 0.50$, $\alpha = 10$, $\gamma_w = 0.1$, and other parameters same as in Figure 2.

are the same as those in Figure 2. To the extent operation at a higher γ is tantamount to operating at a lower α, we notice that the series solution predictive accuracy is somewhat higher than those shown in Figure 3 at comparable cuts. In fact, one can go as far as a cut of $\theta = 0.45$ with little error. Reduction of the γ_w to 0.05 and therefore of p_w to 1.25 atm, on the other hand, is equivalent to increasing α. Thus, we see in Figure 7 somewhat higher errors at the highest $\theta \simeq 0.40$ than those observed in Figure 3, where $\gamma_w = 0.1$, i.e. $p_w = 2.5$ atm, was used.

The feed mole fraction was, so far, fixed at $x_f = 0.209$. When the feed composition is increased to $x_f = 0.50$ in Figure 8 for $\alpha = 10$, all other conditions being similar to those in Figure 3, we observe, as in Figure 3, that the predictive accuracy is quite good up to a cut of $\theta \simeq 0.40$. Thus, changing x_f from 0.209 to 0.5 did not materially affect the range over which the series solutions are accurate. This is further reinforced if we observe the behavior

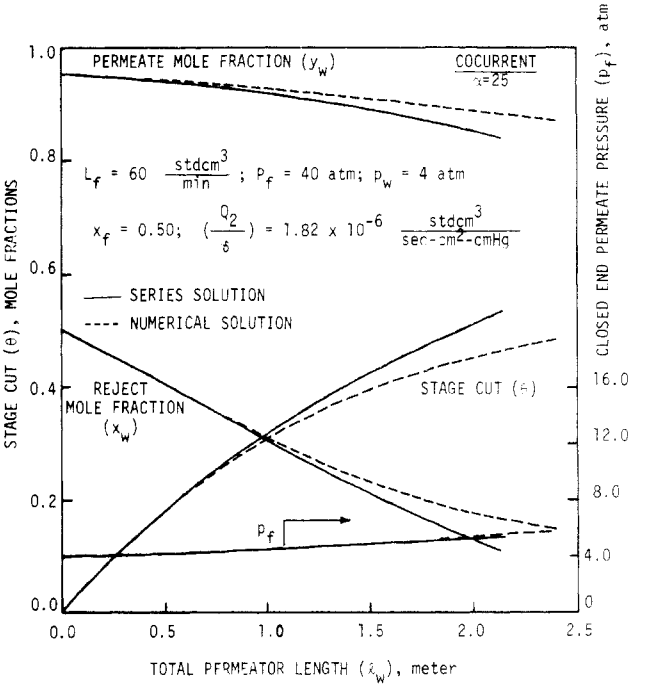

Figure 9. Comparison of series and numerical solutions for cocurrent hollow fiber permeators for $x_f = 0.50$, $\alpha = 25$, $\gamma_w = 0.1$, and other parameters same as in Figure 4.

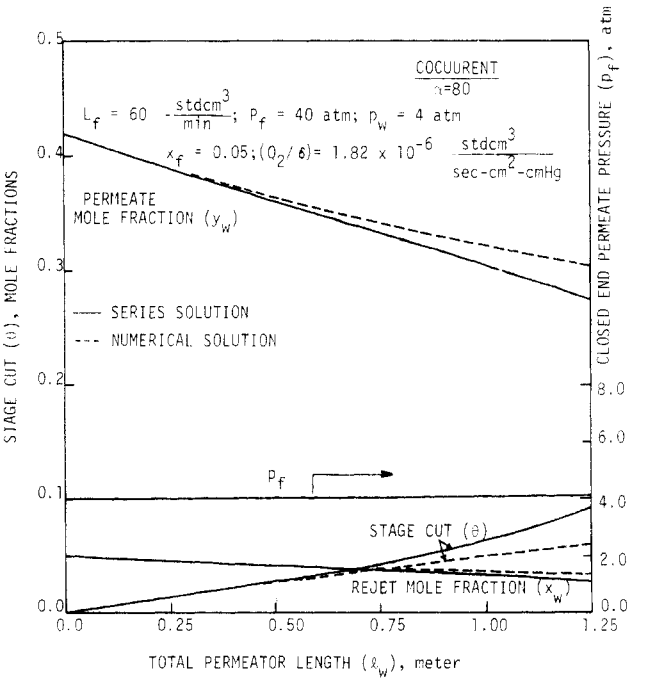

Figure 10. Comparison of series and numerical solutions for cocurrent hollow fiber permeators for $x_f = 0.05$, $\alpha = 80$, $\gamma_w = 0.1$, and other parameters same as in Figure 4.

for $\alpha = 25$, $x_f = 0.50$, and $p_w = 4$ atm ($\gamma_w = 0.1$) in Figure 9 where the series solutions are quite efficient up to a cut of about 0.35. However, when a $x_f = 0.05$ is chosen for $\alpha = 80$ and $p_w = 4$ atm ($\gamma_w = 0.1$), we find from Figure 10 that beyond a cut of $\theta \simeq 0.05$ accuracy is low, unlike that in Figure 5 where accuracy is reasonable up to $\theta \simeq 0.14$. This is somewhat expected since a cut of $\theta \simeq 0.05$ for $x_f = 0.05$, $\alpha = 80$, and $\gamma_w = 0.1$ is quite high. It is to be noted that all conditions in Figures 9 and 10 except x_f and α are exactly the same as those in Figures 4 and 5.

Countercurrent Hollow Fiber Gas Permeators. We next present the results for countercurrent hollow fiber gas permeators using essentially the format followed for co-

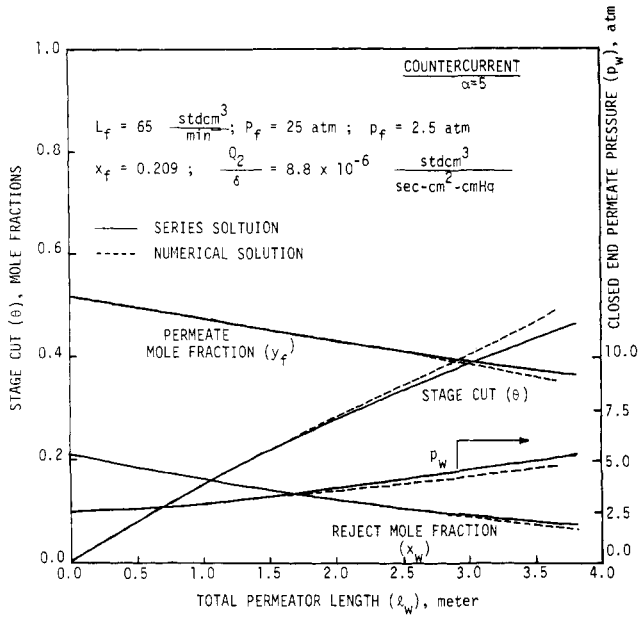

Figure 11. Comparison of series and numerical solutions for countercurrent hollow fiber gas permeators for $x_f = 0.209$, $\alpha = 5$, $\gamma_f = 0.1$, and other parameters same as in Figure 2.

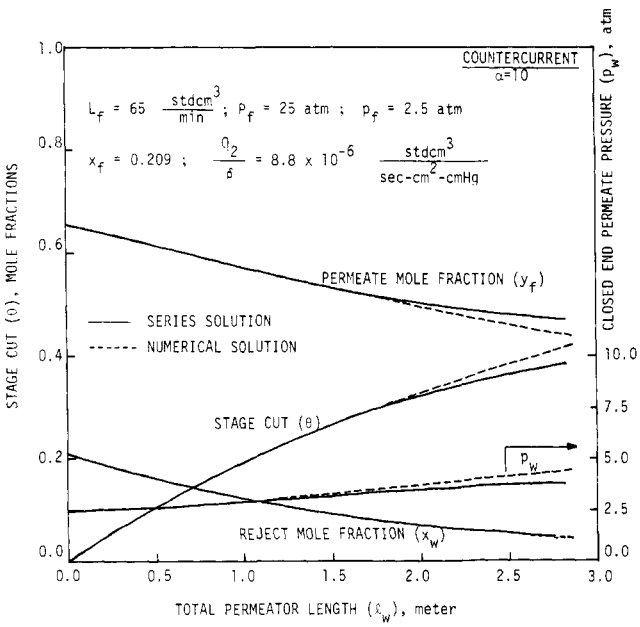

Figure 12. Comparison of series and numerical solutions for countercurrent hollow fiber permeators for $x_f = 0.209$, $\alpha = 10$, $\gamma_f = 0.1$, and other parameters same as in Figure 2.

current permeators. Note, however, that l_w for the following figures starts from the high-pressure reject end. Further, the closed-end permeate pressure p_w is plotted here instead of p_f. As before, solid lines represent series solutions while the dashed lines are obtained from a numerical solution. The curves depict the behavior of y_f, x_w, p_w, and θ against l_w with each l_w representing a different permeator if L_f is fixed. Figure 11 obtained for $\alpha = 5$, $x_f = 0.209$, and $p_f = 2.5$ atm (all other conditions being similar to those of Figure 2) shows that the countercurrent permeators display a behavior very similar to that in cocurrent permeators. The percent errors in y_f and θ at the highest cut of $\theta = 0.47$ at $l_w = 3.8$ m are around 4% and 8%, respectively. Note that the error in countercurrent flow series solution predictions is somewhat higher than in cocurrent flow.

An additional feature worth noting is that the countercurrent permeator is producing a richer permeate, a

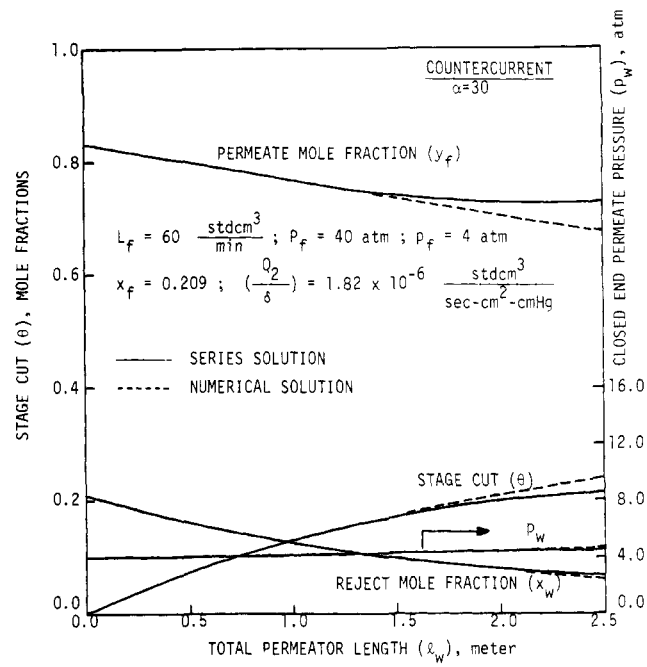

Figure 13. Comparison of series and numerical solutions for countercurrent hollow fiber permeators for $x_f = 0.209$, $\alpha = 30$, $\gamma_f = 0.1$, and other parameters same as in Figure 4.

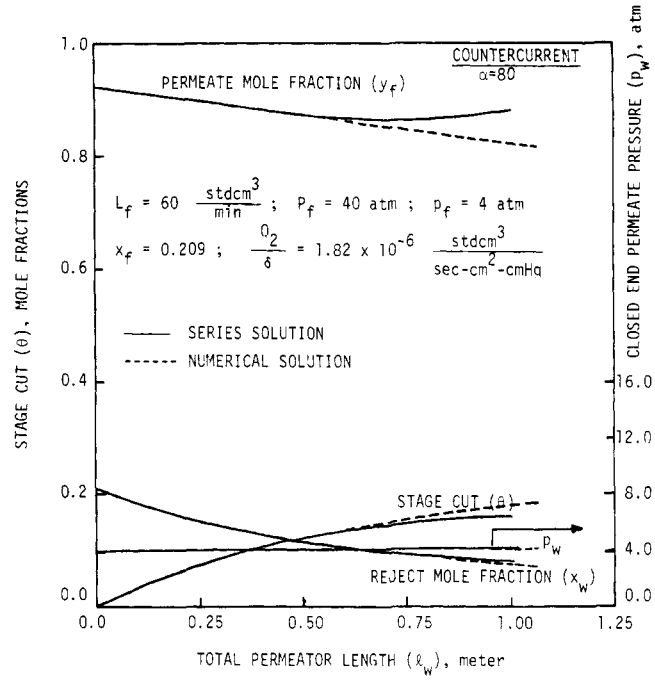

Figure 14. Comparison of series and numerical solutions for countercurrent hollow fiber permeators for $x_f = 0.209$, $\alpha = 80$, $\gamma_f = 0.1$, and other parameters same as in Figure 4.

leaner reject (lower x_w), and a higher cut at the same value of the hollow fiber length, l_w, if the two numerical solutions are compared. Further, any cocurrent permeator has a higher pressure generated at the closed end than that in a countercurrent permeator with the same fiber length, other conditions remaining the same. This feature will be observed in all of our calculations and will be discussed more fully elsewhere.

The efficiency of the series solutions is investigated next in Figure 12 when α is changed to 10, all other conditions remaining the same as in Figure 11. Again, the behavior of the series solution vis-à-vis the numerical solution is very similar to that with cocurrent flow permeators (Figure 3). In fact, the percent errors for the largest permeator (l_w =

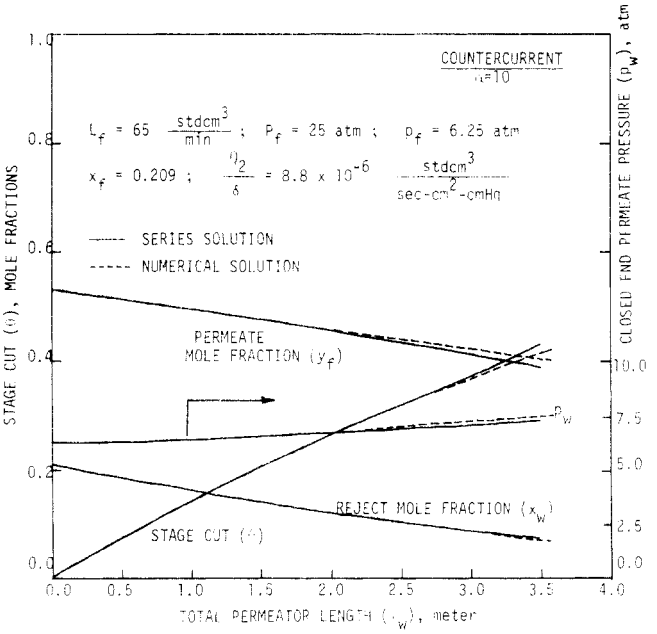

Figure 15. Comparison of series and numerical solutions for countercurrent hollow fiber permeators for $x_f = 0.209$, $\alpha = 10$, $\gamma_f = 0.25$, and other parameters same as in Figure 2.

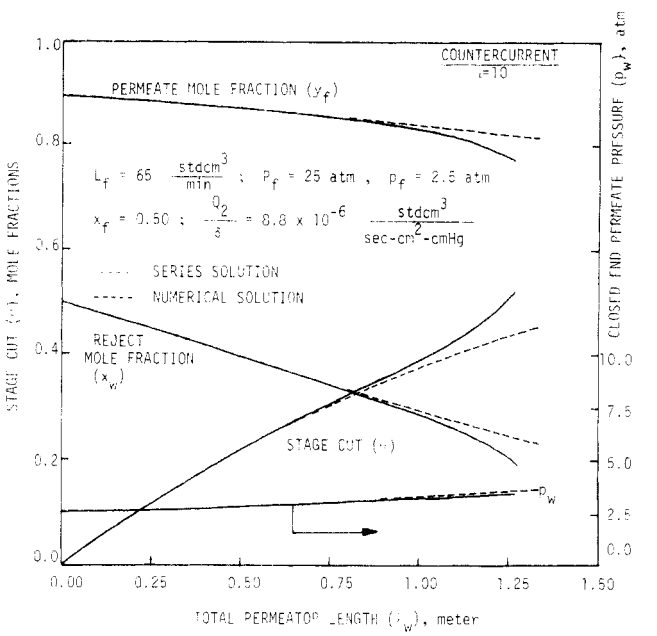

Figure 16. Comparison of series and numerical solutions for countercurrent hollow fiber permeators for $x_f = 0.5$, $\alpha = 10$, $\gamma_f = 0.1$, and other parameters same as in Figure 2.

2.8 m) in y_f and θ are around 7% and 9% with θ around 0.40. Increasing α to 30 for countercurrent permeators (Figure 13) indicates that the series solution accuracy is quite good up to $\theta \simeq 0.24$. Series solution accuracies decrease beyond $\theta \simeq 0.16$ if α is increased to 80 for countercurrent permeators (Figure 14).

Changing the pressure ratio γ_f from 0.1 (Figure 12) to 0.25 and therefore p_f from 2.5 atm to 6.25 atm for $\alpha = 10$ leads to higher predictive accuracies as shown in Figure 15. Thus, the behavior of the series solution for countercurrent flow is essentially similar to that for cocurrent flow (Figure 6) when pressure ratio is increased. Although we are not showing any results here for $\gamma_f = 0.05$, the behavior again is essentially similar to that in cocurrent flow; i.e., for the same conditions, accuracy at a given cut is reduced by decreasing γ.

The effect of a change in feed composition from $x_f = 0.209$ to $x_f = 0.50$ for $\alpha = 10$ and $p_f = 2.5$ atm ($\gamma_f = 0.10$) is shown in Figure 16. As observed in Figure 8 for cocurrent flow, predictive accuracy is quite good up to $\theta = 0.45$. Although we are not showing here any results for countercurrent flow for a low $x_f = 0.05$, the behavior is essentially similar to that observed in cocurrent flow (Figure 10).

Discussion

Preliminary design or rating of a hollow fiber gas permeator with permeate flowing through the fiber lumens and encountering substantial pressure drop can then be carried out by simply solving only algebraic equations. For example, for a cocurrent hollow fiber permeator rating problem, only one algebraic equation has to be solved for unknown γ_f. For a cocurrent hollow fiber design problem, two algebraic equations have to be solved for γ_f and R_{fT}. Similarly, for a countercurrent hollow fiber design problem with x_w specified, two algebraic equations have to be solved for γ_w and R_{wT}. For countercurrent hollow fiber rating problems, three algebraic equations have to be solved simultaneously. However, such solutions can be developed rapidly with a minimum of sophistication about the general hollow fiber gas permeator design or rating problem. It is also clear that such series solutions can predict relevant quantities with reasonable accuracy as long as the cut is not too large. Thus, such solutions are useful for preliminary process design or performance analysis since very high cuts are never encountered in commercial permeators.

An additional aspect needs to be stressed. The structure of a numerical design program for a hollow fiber gas permeator has to be quite different from that for a numerical rating program. No such distinction is necessary for the approximate series solutions developed here. The difference between the various problems lies only in the number of algebraic equations to be solved simultaneously.

Our choice of α and x_f values reflects conditions likely to be encountered in industrial membrane gas processing. For example, O_2–N_2 separation factors through cellulose acetate (CA) or PRISM membranes are around 5–6 with air as feed. Acid gas purification of natural gas (a CO_2–CH_4 system, say) encounters a separation factor of around 25–30 through the same membranes (Mazur and Chan, 1982). Recovery of H_2 from H_2–CO mixtures with the same membranes involves α in the range of 30–40. The separation factor of He–CH_4 or H_2–CH_4 mixtures through similar membranes is around 60–80. Although some of our selections of α–x_f combinations may not be encountered in current industrial practice, they were chosen to reflect a variety of possible conditions.

Figures 2–16 comparing the series solution with the numerical solution do not indicate the composition, pressure, or cut profiles along a permeator of the highest membrane length shown. To obtain the composition, pressure, and cut profiles along a permeator of given dimensions (i.e., given l_w or R_{fT}), say, for cocurrent flow, solve for γ_f for given x_f and γ_w from eq 42 and then obtain directly the new values of x, y, and γ for smaller permeators, with increasingly smaller values of R_f from eq 24, 25, and 26, respectively, with the given x_f and the value of γ_f determined above. Similarly, for a countercurrent permeator with given l_w, solve for γ_w, x_w, and y_f from eq 59–61 for the given x_f and γ_f. With L_w being known now, select different values of l for the same L_w to obtain different and smaller values of R_w smaller than that used earlier. Now use eq 43, 44, and 45 respectively to obtain from the left-hand sides values of x, y, and γ for each l (therefore R_w) and γ_w determined already. These will provide the local values at the corresponding location in

the original permeator whose x_f, x_w, and γ_w are to be used for calculations on the right-hand sides of eq 43–45.

Differences in separation capabilities of a hollow fiber gas permeator with flow patterns exist for almost all combinations of parameters investigated here. However, for not too high a cut, the differences are not drastic. Therefore, for preliminary or shortcut procedures, one may adopt the solution to the cocurrent rating problem suggested here involving the solution of only one algebraic equation for γ_f. A set of values of γ_f for different l_w–s or R_{fT}–s for specified γ_w, x_f, and α will allow one to easily carry out a cocurrent design or rating problem over a range of conditions. Nothing more than a hand-held programmable calculator would be necessary.

Acknowledgment

N. Boucif acknowledges with thanks the financial support of Sonatrach DRD/END, 16 Rue Sahara, Hydra, Algiers, Algeria, through its scholarship award.

Appendix. Design Approach for Permeators of Given Length

Until now, our analyses have tacitly assumed that the feed flow rate is a constant. Therefore, in a design problem, one has to determine the fiber length l_w for either a given reject composition x_w or a given permeate composition (y_w for cocurrent flow, y_f for countercurrent flow). Often hollow fiber modules are produced with a few fixed lengths. Thus, l_w is fixed from considerations of modules practically available. Finding the feed flow rate per fiber, L_f, then becomes the design objective instead of finding l_w. Since β in the pressure drop equations (3) and (14) is a function of L_f, which is now unknown, an alternate procedure described below has to be adopted.

Define a new dimensionless quantity ϕ as

$$\phi = \frac{256(Q_2/\delta)D_{lm}l_w^2\mu RT}{D_i^4 P_f} \tag{A1}$$

so that for cocurrent flow

$$\beta = \phi/R_{fT}^2 \tag{A2}$$

and for countercurrent flow

$$\beta = \phi\left[\left(\frac{y_f - x_w}{y_f - x_f}\right)^2 \Big/ R_{wT}^2\right] \tag{A3}$$

Note that for any design problem with fixed l_w, P_f, D_i, D_{lm}, and Q_2/δ, ϕ is fixed and therefore a constant. For *cocurrent flow*, it follows easily from inspection that the coefficients b_2, c_2, a_3, b_3, and c_3 become additionally dependent on R_{fT} since they are each dependent on β (which depends on R_{fT} by eq A2). However, the design procedure does not change. If x_w is given, solve eq 40 and 42 simultaneously for the two unknowns, γ_f and R_{fT}, as before. The quantity y_w may be calculated next from eq 41. If y_w is given, solve eq 41 and 42 for γ_f and R_{fT}, as before, and calculate x_w afterward. Once R_{fT} is determined, L_f can be directly obtained and the number of fibers or modules in parallel determined for any given total feed flow rate.

For countercurrent flow with given x_w, the design procedure, however, changes somewhat since now the coefficients e_2, f_2, d_3, e_3, and f_3 become dependent not only on R_{wT} but also on y_f. Thus, one has to solve, simultaneously, three algebraic equations (59) to (61) for unknowns γ_w, R_{wT}, and y_f (compared to two algebraic equations earlier). Using eq 58, one can then obtain L_f since R_{wT} and y_f are known.

For countercurrent flow with given y_f, the mode of solution remains as before, except the dependence of some of the coefficients in terms of R_{wT} and x_w has to be used explicitly via relation A3.

Nomenclature

A = constant defined by eq 61a and 49c
a_0, a_1, a_2, a_3 = coefficients in expansion 24 defined by eq 27, 32, 35, and 38, respectively
B = constant defined by eq 61a and 49d
b_0, b_1, b_2, b_3 = coefficients in expansion 25 defined by eq 31, 34, 36, and 39, respectively
c_0, c_1, c_2, c_3 = coefficients in expansion 26 defined by eq 28, 33, 37, and 39a, respectively
D_i, D_o, D_{lm} = inside, outside, and log mean diameters of hollow fiber, respectively
d_0, d_1, d_2, d_3 = coefficients in expansion 43 defined by eq 46, 48, 52, and 56, respectively
e_0, e_1, e_2, e_3 = coefficients in expansion 44 defined by eq 49, 51, 54, and 57, respectively
f_0, f_1, f_2, f_3 = coefficients in expansion 45 defined by eq 47, 50, 53, and 55, respectively
L = molar flow rate of high-pressure gas at a given permeator location
l, l_w = active length of hollow fiber at any permeator location and total active length, respectively
P_f = pressure of high-pressure gas
p = pressure of low-pressure gas inside hollow fiber at any permeator location
Q_1, Q_2 = permeability of more permeable species 1 and the less permeable species 2, respectively
R_f = nondimensional membrane area for cocurrent permeator defined by eq 4a at a given permeator location
R_f^{cc} = nondimensional membrane area for countercurrent permeator defined by eq 15 at a given permeator location
R_w = nondimensional membrane area for countercurrent permeator defined by eq 15 at a given permeator location
T = absolute temperature
V = molar flow rate of low-pressure gas at a given permeator location
x, x_f, x_w = mole fraction of more permeable species 1 in high-pressure gas at any permeator location, feed entry, and residue exit locations, respectively
y, y_f, y_w = mole fraction of more permeable species 1 in low-pressure permeate gas inside hollow fibers at any permeator location, feed entry, and residue exit locations, respectively

Greek Letters

α = ideal separation factor, defined by eq 4
β = constant for pressure drop equations, defined by eq 4c
γ = local pressure ratio, defined by eq 4
δ = thickness of nonporous membrane
μ = viscosity of permeate gas
θ = permeator cut defined by eq 9 or 11 for cocurrent permeator and by eq 21 or 23 for countercurrent permeator
ϕ = constant defined by eq A1

Subscripts

f = pertaining to the permeator axial location where high-pressure feed enters
T = total value, used for permeator membrane area
w = pertaining to the permeator axial location where high-pressure feed exits

Superscript

cc = pertaining to countercurrent permeator with calculations beginning at high-pressure reject end

Literature Cited

Antonson, C. R.; Gardner, R. J.; King, C. F.; Ko, D. Y. *Ind. Eng. Chem. Process Des. Dev.* **1977**, *16*, 473.
Boucif, N.; Majumdar, S.; Sirkar, K. K. *Ind. Eng. Chem. Fundam.* **1984**, *23*, 470.

Chern, R. T.; Warrick, M.; Fedkiw, P. F.; Koros, W. J. Presented at the Winter National Meeting of American Institute of Chemical Engineers, Atlanta, GA, March 14, 1984; paper 30a.
Maclean, D. L.; Graham, T. E. *Chem. Eng.* **1980**, *25*, 54.
Mazur, W. H.; Chan, M. C. *Chem. Eng. Prog.* **1982**, *78*, 38.
Pan, C. Y.; Habgood, H. W. *Can. J. Chem. Eng.* **1978**, *56*, 210.
Pan, C. Y. *AIChE J.* **1983**, *29*, 545.
Pereyra, V. *Lecture Notes Comp. Sc. 76*; Springer-Verlag: West Berlin, 1978; pp 67-88.
Sengupta, A.; Sirkar, K. K. *J. Membr. Sci.* **1984**, *21*, 73.
Stern, S. A.; Onorato, F. J.; Libove, C. *AIChE J.* **1977**, *23*, 567.
Thorman, J. M.; Rhim, H.; Hwang, S. T. *Chem. Eng. Sci.* **1975**, *30*, 751.

Received for review March 30, 1984
Accepted June 2, 1985

This material was presented in part at the Symposium on Gas Separation by Membranes at the Winter National AIChE Meeting, Atlanta, GA, March 14, 1984.

Optimal Feed Distribution in Reactions with Maximal Rate

Moshe Sheintuch,* Ovadia Lev, Shlomo Mendelbaum, and Benny David

Department of Chemical Engineering, Technion-Israel Institute of Technology, Haifa 32000, Israel

Solutions for the optimal locations and flow rates of N feed side streams into a tubular reactor are derived for the case of a nonmonotonic rate expression. Application of these criteria for a Langmuir-Hinshelwood expression exhibits a significant reduction in the required volume of an isothermal reactor and an order of magnitude decrease when the reactor is isothermal. Mass-transfer resistance effects are also analyzed. The proposed scheme is superior to mixing and/or subsurface catalyst deposition since it is simpler mechanically and free from problems of steady-state multiplicity.

Introduction

One of the early lessons of the basic course in reaction engineering is the comparison of the residence times required to achieve a specified conversion in a plug-flow reactor (PFR) and a continuous stirred-tank reactor (CSTR). We owe it to Levenspiel's textbook (1972) that the graphical construction in the inverse rate vs. concentration plane clearly demonstrates that the PFR (CSTR) is superior when the rate is a monotonically increasing (decreasing) function. Yet, the CSTR is not always the best design for a reaction with negative-order kinetics. Such a rate expression, $r(C)$, exhibits a local maximum since $r(0) = 0$, and the optimal design is one that operates at the maximal rate, r_M, for most or all of the reactor length. That usually poses a technical problem since mixing, stirring, or recycling requires investment in mechanical devices and energy. The same effect, however, can be achieved by proper distribution of the feed along the reactor. We explore here the optimization of such a distribution.

The incentive for this work originates in the design of the automobile catalytic converter where effluent recycling is not feasible. The source of the maximal rate in the monolith, or in any catalytic reactor, is due to either reactant inhibition or temperature (product) acceleration in an adiabatic reactor. Reactant inhibition effects are evident in CO, NH_3, olefins, and alcohol oxidation reactions as well as in methanation and Fischer-Tropsch reactions. The isothermal rate expressions for these reactions are classified by Harold et al. (submitted) according to the following hierarchy: nonmonotonic single-valued (e.g., Figure 1a), continuous multivalued (Figure 1d), and discontinuous. For simplicity we focus attention on continuous, single-valued intrinsic rate curves with local maxima and comment later on the effect of multiplicity. The most commonly employed rate function in that category is the explicit Langmuir-Hinshelwood expression

$$r = \frac{kC}{(1 + KC)^2}; \quad k = k_0 \exp\left(-\frac{E}{RT}\right); \quad K = K_0 \exp\left(-\frac{\Delta H_a}{RT}\right) \quad (1)$$

Note that when adsorption equilibrium is not assumed in a Langmuir-Hinshelwood mechanism, the rate may still show negative-order kinetics even though the rate expression may not be represented by an explicit formula. Nonetheless, the proposed optimal solution can be derived graphically and may be applied.

A thermal acceleration effect exists in all of the reactions mentioned above as well as in any exothermic nth-order reaction carried out in an adiabatic reactor (e.g., the catalytic oxidation of paraffins). The apparent rate then follows the expressions

$$r = k_0 C^n \exp\left(-\frac{E}{R}\left(\frac{1}{T} - \frac{1}{T_0}\right)\right); \quad T = T_0 + \Delta T_a(1 - C/C_0) \quad (2)$$

Biochemical and enzymatic reactions may acquire a maximal rate due either to substrate (reactant) inhibition, usually modeled by

$$r = \frac{kS}{K_s + S + S^2/K_I} \quad (3)$$

or to acceleration by a product microorganism, expressed as

$$r = \mu(S)X; \quad X = X_0 + Y(S_0 - S) \quad (4)$$

Expressions 1-3 are of the form shown in Figure 1a, and eq 4 acquires a local maximum even when $\mu(S)$ is monotonic, as in Figure 1b.

In the rate expressions above we have assumed the existence of a single limiting reactant; the temperature-concentration relation (eq 2) and the substrate-biomass concentration relation (eq 4) are uniquely determined when a single reaction exists and are independent of the flow distribution. A constant density of the reacting phase is assumed for simplicity.

The main result, the procedure for deriving the optimal feed distribution, is underlined at the beginning of the next section. The example of the catalytic converter is presented in the second section. The following section presents the advantages of the proposed scheme over other optimal strategies such as subsurface catalyst impregnation or

0196-4313/86/1025-0228$01.50/0